2007 GCEP Report

Project title: Advanced Materials and Devices for Low Cost and High Performance Organic Photovoltaic Cells

Investigators

Zhenan Bao, Associate Professor, Chemical Engineering

Mike McGehee, Assistant Professor, Material Sciences and Engineering

Toshihiro Okamoto, Nobuyuki Miyaki, Alex Mayer, Postdoc Researchers; Ming Lee Tang, Ying Jiang, Quan Yuan, Colin Reese, Shawn Ryan Scully, George Burkhard, Graduate Researchers

Abstract

Exciton harvesting is of fundamental importance for the efficient operation of organic photovoltaic devices. The quantum efficiencies of many organic and hybrid organic-inorganic devices are still limited by low exciton harvesting efficiencies. This problem is most apparent in planar heterostructures that suffer from a direct tradeoff between light absorption and exciton harvesting. One approach to overcome small diffusion lengths is the use of triplet excitons. We have an ongoing project investigating pentacene/C60 solar cells to determine if triplets are the dominant exciton species following photoexcitation. Simulations of exciton harvesting suggest that excitons in pentacene are triplets. These triplets are likely formed by an exciton fission route which further has implications for beating the Shockley-Queisser limit and experiments are ongoing to verify this.

In addition to using triplets to harvest excitons over long distances, we have developed a new scheme using long range resonant energy transfer to harvest singlet excitons over 25 nm away from the donor-acceptor interface in organic solar cells using resonant energy transfer. These results represent dramatic improvements over our previous findings and show that this scheme holds promise for the future design of highly efficient organic photovoltaics. We present theory and experiment demonstrating a scheme to harvest singlet excitons over 25 nm away from a donor-acceptor interface using resonant energy transfer. Improvement in materials choice could yield effective diffusion lengths as large as 40 nm using long-range transfer, while minimizing the energy loss to less than 0.1 eV making this a promising approach for developing highly efficient organic photovoltaics.

Finally, we have successfully synthesized several new low-band gap polymers. Several of these polymers have bandgap of 1.7 eV or lower. Evaluation of the performance of these new materials is underway.

Introduction

A significant fraction of the carbon released into the atmosphere is a result of burning coal and natural gas to produce electricity. It is therefore highly desirable to find ways to generate electricity without releasing carbon. The development of affordable photovoltaic (solar) cells is one of the most promising long-term solutions to keeping the CO_2 concentration in the atmosphere at safe levels.

Currently, almost all photovoltaic (PV) cells being manufactured are made of crystalline silicon. The average cost of the electricity that is generated in a sunny location using these cells is about two-four times more than the typical cost of electricity from the grid. Our goal is to develop technology that can reduce the cost per Watt of generation capability by at least a factor of five and hopefully even more. Our approach is to use organic semiconductors because they can be deposited onto flexible substrates in roll-to-roll coating machines, similar to those used to make photographic film and newspapers. In this project, we plan to work on three directions: (i) having significant exciton harvesting and preventing geminate recombination by using phosphorescent semiconductors, (ii) new device designs and materials required for double or triple the efficiency, and (iii) new materials design concepts to improve the absorption of low energy photons by using new low band gap semiconductors that have sufficient charge carrier mobilities for charge extraction.
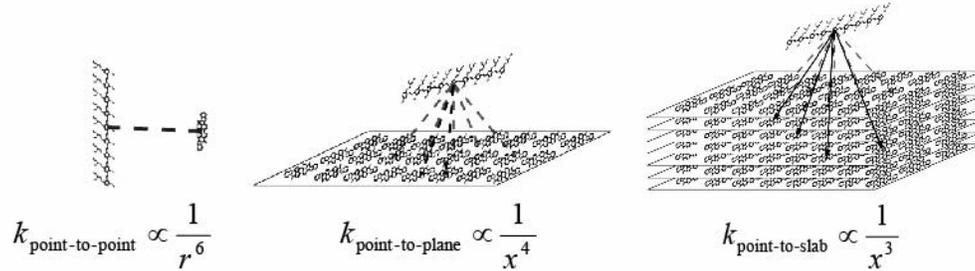
Results

Enhanced Exciton Harvesting through Long Range Resonant Energy Transfer

Exciton harvesting is of fundamental importance for the efficient operation of organic photovoltaic devices. The quantum efficiencies of many organic and hybrid organic-inorganic devices are still limited by low exciton harvesting efficiencies. This problem is most apparent in planar heterostructures that suffer from a direct tradeoff between light absorption and exciton harvesting. One approach to overcome small diffusion lengths we've already discussed is the use of triplet excitons. We have also developed a new scheme using long range resonant energy transfer to harvest singlet excitons over 25 nm away from the donor-acceptor interface in organic solar cells using resonant energy transfer. These results represent dramatic improvements over previous findings[4] and show that this scheme holds promise for the future design of highly efficient organic photovoltaics.

Resonant energy transfer has been used in organic photovoltaics to broaden the absorption spectrum and is thought to play a role in harvesting excitons in bulk heterojunction cells. However, the intentional use of hetero-energy transfer to achieve longer range exciton harvesting in photovoltaics had largely been overlooked until recently [4]. Since the rate of transfer between two chromophores is proportional to $1/r^6$ and the characteristic distance of transfer is typically only 2-4 nm, it is often assumed that, at best, excitons could be harvested across this marginally larger distance when energy transfer is used. However, both the relevant geometry and a proper accounting of rates

are of the utmost importance in determining absolute transfer rates. In a heterostructure, the exciton in the donor phase can be transferred to any one of the chromophores in the acceptor film. Therefore, to obtain the total rate of transfer we must sum over all possible transfer events. This is shown schematically in Figure 1.

$$k_{\text{point-to-point}} \propto \frac{1}{r^6} \qquad k_{\text{point-to-plane}} \propto \frac{1}{x^4} \qquad k_{\text{point-to-slab}} \propto \frac{1}{x^3}$$

Figure 1. Schematics showing representations of three different geometries for energy transfer, point-to-point (left), point-to-plane (center), and point-to-slab (right). For simplicity, only the excited chromophore is drawn on the donor side, while in physically relevant systems the excited chromophore is embedded in a 3-D matrix of non-excited donor chromophores. Small D-A separation distances were chosen to emphasize the various possible transfer pathways. At larger distances (>10 nm) the donor would look like a point and the acceptor planes and slabs would appear to be continuous rather than discrete as above. The arrows show representative energy transfer pathways. Point-to-point corresponds to the situation where both donor and acceptor chromophores are randomly dispersed in a matrix. Point-to-plane corresponds to the case where a donor chromophore can couple to a monolayer of acceptor molecules. Point-to-slab corresponds to the case where a donor chromophore can couple to a 3-D array of acceptor molecules.

The rate of transfer from an excited chromophore to a 2-D sheet varies as $1/x^4$ [5] and to a 3-D seminfinite array as $1/x^3$ [5, 6], where x has been chosen as a distance from a planar interface rather than a radial distance. Energy transfer for the geometrically relevant structures is many times more efficient than would be the case between two isolated chromophores.

We have reported device results using regioregular poly(3-hexylthiophene (RR-P3HT) as the energy donor and the low bandgap polymer poly(N-dodecyl-2,5,-bis(2'-thienyl)pyrrole-2,1,3-benzothiadiazole) (PTPTB) as the energy acceptor[4]. We showed a near threefold enhancement in the photocurrent compared to a titania/RR-P3HT bilayer device and exciton harvesting measurements showed that excitons could be harvested from nearly 10 nm away from the heterointerface. RR-P3HT is well-known to have a low luminescence quantum yield due to tight pi-pi stacking and efficient aggregate/excimer formation that limits the usefulness of resonant energy transfer in this system by reducing the Förster radius. We will now quantitatively explain exciton harvesting using hetero-energy transfer and show simulations and experiments that demonstrate dramatic improvements upon these early results.

Exciton migration is usually modeled assuming a random walk, perfect quenching at the donor-acceptor interface, and perfect reflecting at the non-quenching interface. For the 1-D case, the continuity equation for the exciton density, n, and the idealized boundary conditions are given in Equations 1.1-1.3.

$$\frac{\partial n}{\partial t} = D\frac{\partial^2 n}{\partial x^2} - \frac{n}{\tau} + G(x)$$

(1.1)

$$n\big|_{quench} = 0$$

(1.2)

$$-D\frac{\partial n}{\partial x}\bigg|_{nonquenching} = 0$$

(1.3)

The first term on the right in Equation 1.1 corresponds to exciton diffusion with diffusivity, D. The second term is the natural decay of the exciton with lifetime τ and the third is the exciton generation profile, $G(x)$. Equation 1.2 is the boundary condition for a perfectly quenching interface (which the D-A heterointerface ideally acts as) whereas Equation 1.3 is the condition for a perfectly reflecting interface. As alluded to earlier, because of disorder, singlet migration is not actually a true random walk. Consequently "exciton diffusion" is a misleading term. However, it turns out that steady-state exciton harvesting measurements can still be well-described using this model and an effective diffusion length, $L_D = \sqrt{D\tau}$, can be extracted that consistently models exciton harvesting in a variety of experiments. In this way L_D is more of an empirical factor that describes average exciton migration properties. When the spatial generation of excitons is a constant, an organic film with thickness equal to L_D will have an exciton harvesting efficiency of about three quarters when a donor-acceptor interface is present at one of the surfaces of the organic film.

Following this empirical spirit, we can simulate exciton harvesting when hetero-energy transfer is possible as an additional exciton migration pathway. Equation 2.1 is a modified continuity equation, which includes an extra term corresponding to exciton harvesting by long-range resonant energy transfer with the rate given by Equation 2.2.

$$\frac{\partial n}{\partial t} = D\frac{\partial^2 n}{\partial x^2} - \frac{n}{\tau} - k_F \cdot n + G(x)$$

(2.1)

$$k_F(x) = \frac{C_A}{\tau}\frac{\pi}{6}\frac{R_o^6}{x^3}$$ (2.2)

where Ro is the Förster radius and C_A is the acceptor chromophore densityCA is the acceptor chomophore density which is also used in the calculation of Ro, since Ro depends on the molecular absorptivity. Presented a different way we could show that the rate depends only on the total absorption coefficient. As formulated CA must be consistently used in this equation and in the calculation of Ro. We choose 8/nm3. . Equation 2.1 is numerically solved to calculate the fraction of excitons harvested as described previously using the same boundary conditions as 1.2-1.3.
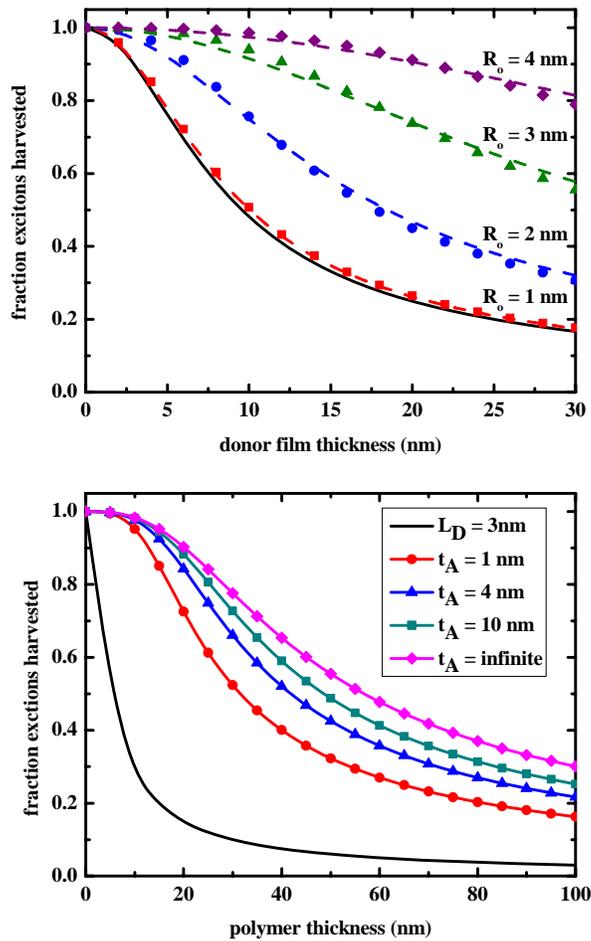
Figure 2 a.) Simulations of the fraction of excitons harvested vs. energy donor film thickness for diffusion-only with a diffusion length of 5 nm (solid black line) as well as diffusion plus hetero-energy transfer with Förster radii of 1 nm (red squares), 2 nm (blue circles), 3 nm (green triangles), and 4 nm (purple squares). Dashed lines are simulations incorporating effective diffusion lengths of 5.2 nm (red), 9.6 nm (blue), 18.8 nm (green) and 35.5 nm (purple). b.) Simulations showing the effect of varying the energy acceptor film thickness. Curves are shown for diffusion only with LD = 3 nm (solid black curve), and for acceptor film thicknesses of 1 nm (circles), 4 nm (triangles), 10 nm (squares), and infinite thickness (diamonds) all for Ro = 4 nm.

Figure 2a shows exciton harvesting as a function of energy donor film thickness assuming a constant generation rate, and an exciton diffusion length of 5 nm. Curves are shown for the case where there is only exciton diffusion as well as for cases involving energy transfer in addition to intrinsic exciton diffusion. An important parameter, which determines the shape of these curves is the Förster radius, Ro. The Förster radius is a measure of the strength of coupling between donor and acceptor chromophores. Stronger coupling results in a larger Ro and consequently a greater fraction of excitons harvested at large distances. As a means of comparison between intrinsic migration and exciton harvesting via long range energy transfer, we can introduce the concept of an "effective diffusion length."[6] Each of the exciton harvesting data sets surprisingly can be well-fit with a model incorporating only exciton diffusion whereby an effective diffusion length can be extracted.

When Ro is 1 nm, energy transfer leads to very little enhancement in exciton harvesting relative to that of intrinsic diffusion with a diffusion length of 5 nm. Consequently, the effective diffusion length for this system is nearly the same as the intrinsic diffusion length. However, if the Förster radius is 2 nm, the effective diffusion length increases to nearly 10 nm, which is close to the value found in the P3HT/PTPTB system we previously investigated [8]. At Ro = 3 nm, the effective diffusion length is almost 19 nm and for Ro = 4 nm, the effective diffusion length is almost 36 nm, more than seven times the intrinsic diffusion length. This last case is clearly much larger than just the sum of the intrinsic diffusion length (5 nm) and the Förster radius (4 nm). Adding all pairwise rates between excited donor and possible acceptor chromophores predicts the large enhancement in transfer rate compared to that for one pair of donor and acceptor chromophores.

To experimentally demonstrate efficient long-range energy transfer, we have chosen a highly efficient red emitting polymer, DOW Red, as the energy donor and a highly absorptive low bandgap polymer, a recently reported PTPTB-derivative, poly(N-hexadecan-2-yloxycarbonyl-2,5-bis(2'-thienyl)pyrrole-2,1,3-benzothiadiazole), as the energy acceptor [9]. This PTPTB-derivative was designed to have thermally labile solubilizing groups, which made it ideally suited for use in heterostructures since a thin film could be deposited from solution and made insoluble by a simple heat treatment. In this way, well-defined heterostructures with no layer interpenetration could be produced. Figure 1a shows normalized photoluminescence and absorption spectra for the two materials. Using these spectra and assuming a 70% luminescence efficiency for DOW Red and random orientation of the donor and acceptor dipoles, we calculate a Förster radius[10] of 3.7 nm and an effective diffusion length of 27 nm.

Exciton harvesting as a function of donor film thickness was measured by comparing the DOW Red photoluminescence on glass, where no exciton harvesting occurs, on titania, where excitons are harvested only by intrinsic migration and subsequent electron transfer at the DOW Red/titania interface, and finally on thin films of the energy acceptor PTPTB which can also harvest excitons through long range energy transfer. The fraction of excitons harvested is given simply by:

$$\eta_{exciton} = \frac{PL_{glass} - PL_{quench}}{PL_{glass}}$$ (3.1)

where PLglass and PLquench are the integrated photoluminescence spectra on glass and quenching substrates respectively. Care was taken to avoid overwhelming interference effects as these can dominate the measurement as we have previously shown[6, 11].
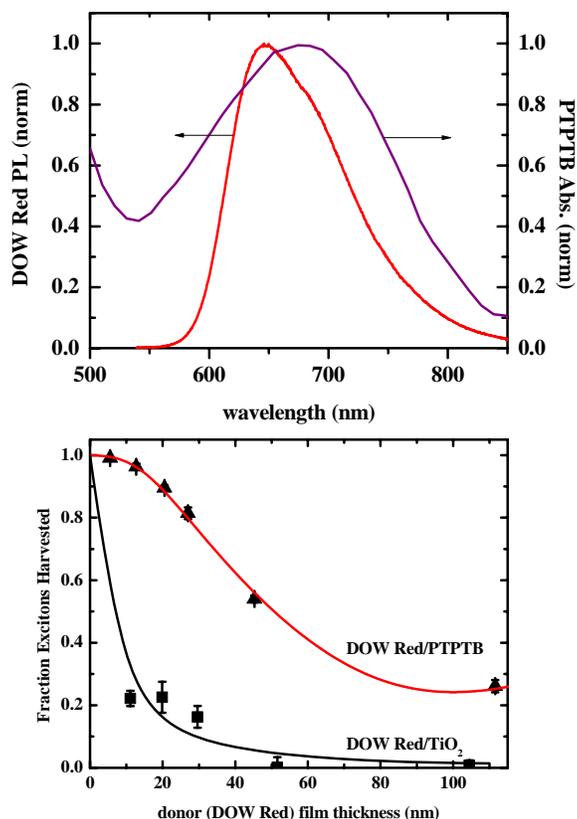
Figure 3. a.) Photoluminescence and absorption spectra of energy donor (Dow Red) (red line) and energy acceptor (PTPTB) (dashed purple line) showing the strong overlap between the two. b.) Fraction of excitons harvested versus DOW Red film thickness on energy acceptor PTPTB (black triangles) and on the wide bandgap electron acceptor TiO2 (black squares). The lower black curve is a simulation corresponding to a diffusion length of 3 nm. The upper red curve is a simulation assuming an effective diffusion length of 27 nm which indicates the superior exciton harvesting when long range energy transfer is possible.

Figure 3 shows exciton harvesting data for DOW Red on titania and for DOW Red on PTPTB. It is clear that more excitons are harvested when PTPTB is incorporated. The continuous curves are models generated from the solutions to Equations 1.1-1.3 assuming a 3 nm (DOW Red on titania) and 27 nm (DOW Red on PTPTB) effective diffusion lengths. These simulations also take into account the optical interference effects that make the generation rate deviate mildly from a constant[6]. In this system, the intrinsic migration of excitons in DOW Red is extremely limited, as is evidenced by the quenching data on titania, which fits a model incorporating only a 3 nm diffusion length. This is in great contrast to the case where energy transfer can occur. When PTPTB is used as a quencher, more than 50% of the excitons created in a 50 nm film are harvested to a planar interface and about 90% of the excitons are harvested in a 20 nm film. In this system, when energy transfer can occur and there is strong coulomb coupling, the effective diffusion length is increased by nearly an order of magnitude.

Because all excitons transferred to the energy acceptor must ultimately migrate back to the donor-acceptor interface where they may be split, it is important to investigate

the influence of exciton harvesting on energy acceptor film thickness. Figure 3b shows simulations of exciton harvesting for different acceptor film thicknesses.

The solid black curve corresponds to intrinsic diffusion with a diffusion length of 3 nm. Simulations are also shown when energy transfer is included and the energy acceptor film thickness is 1 nm (red w/filled circles), 4 nm (blue w/filled triangles), 10 nm (cyan w/filled squares), and infinite (purple w/filled diamonds) thickness. The largest enhancement is seen between the simulation of diffusion only and the simulation incorporating energy transfer with a 1 nm thick acceptor layer. Further enhancement is seen, particularly at larger donor film thicknesses, upon increasing the value of the acceptor film thickness to 4 nm and more to 10 nm, which is not far from the predictions of an infinitely thick acceptor film. This demonstrates that the first few monolayers of the energy acceptor film are the most important, and shows that a surface modification scheme whereby the energy acceptor is placed only at an interface to enhance exciton harvesting is potentially a viable approach to engineer better exciton harvesting in ordered bulk heterojunction cells using an inorganic scaffold.

We have also considered the amount of energy lost during the exciton harvesting process when incorporating Förster transfer since any loss in energy during the processes between exciton photogeneration and charge carrier extraction in a photovoltaic device directly reduces the maximum achievable photovoltage. Since the absorption spectrum of the acceptor must overlap the emission spectrum of the donor, we argue that incorporating long range energy transfer leads to a lowering of the maximum achievable photovoltage by roughly the difference between absorption and emission energies of the donor material. As exemplified by rigid molecules like the acenes and some ladder polymers, this energy loss can be as low as 0.1 eV[12, 13].

We have fabricated various planar heterojunction solar cels (DOW Red/PTPTB and MEH-PPV/PTPTB). In these systems highly efficient exciton harvesting is seen through photoluminescence quenching experiments, but devices show extremely low (<1%) external quantum efficiencies. These quantum efficiencies are even lower than in planar MEH-PPV/TiO2 devices where only intrinsic exciton migration can occur and no long range energy transfer is possible. The quantum efficiencies of these devices are low because of the small HOMO offsets between the energy donor and the energy acceptor. Further improvements will surely come by fabricating donor-acceptor heterostructures with well-defined interfaces, proper heterojunction energetics, and through the choice of donor materials with higher photoluminescence efficiencies.

Low Bandgap Materials and Solar Cells

We have developed general synthetic processes to prepare several new classes of low band-gap polymers. The chemical structures of the polymers are shown in Figure 4. The electrochemical and optical absorption of these polymers are summarized below. Notably, several of the new polymers have bandgap of 1.7 eV and below. We are completing the basic characterizations and optimizing the reaction conditions for these polymers and scaling up the reactions so that we can thoroughly evaluate the solar cell
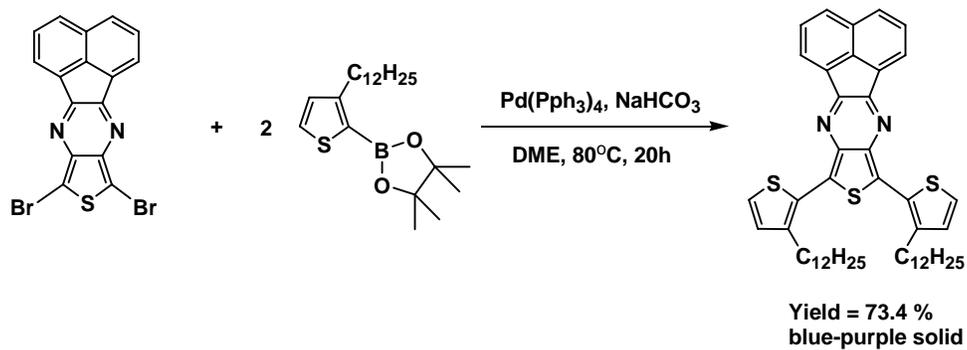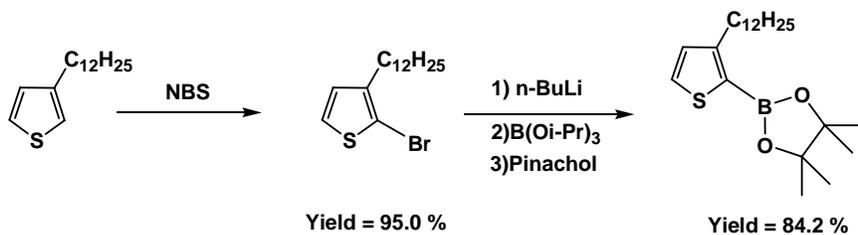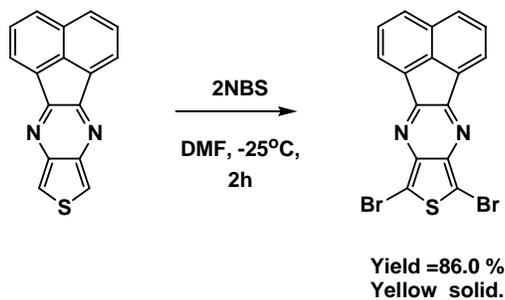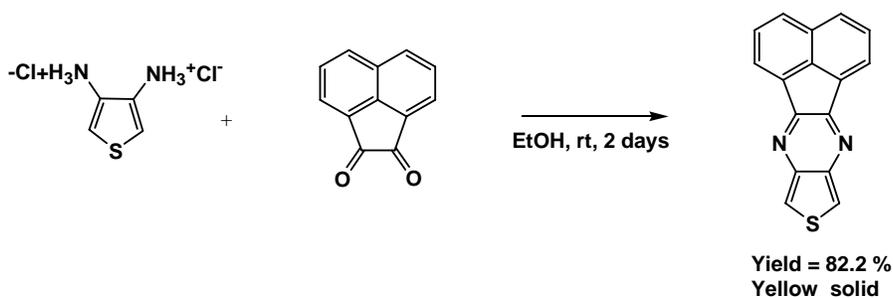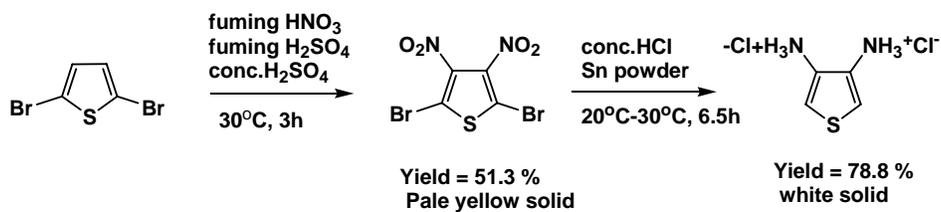
performance of these new polymers. We have performed preliminary solar cell evaluation of **polymer 2** as discussed below.
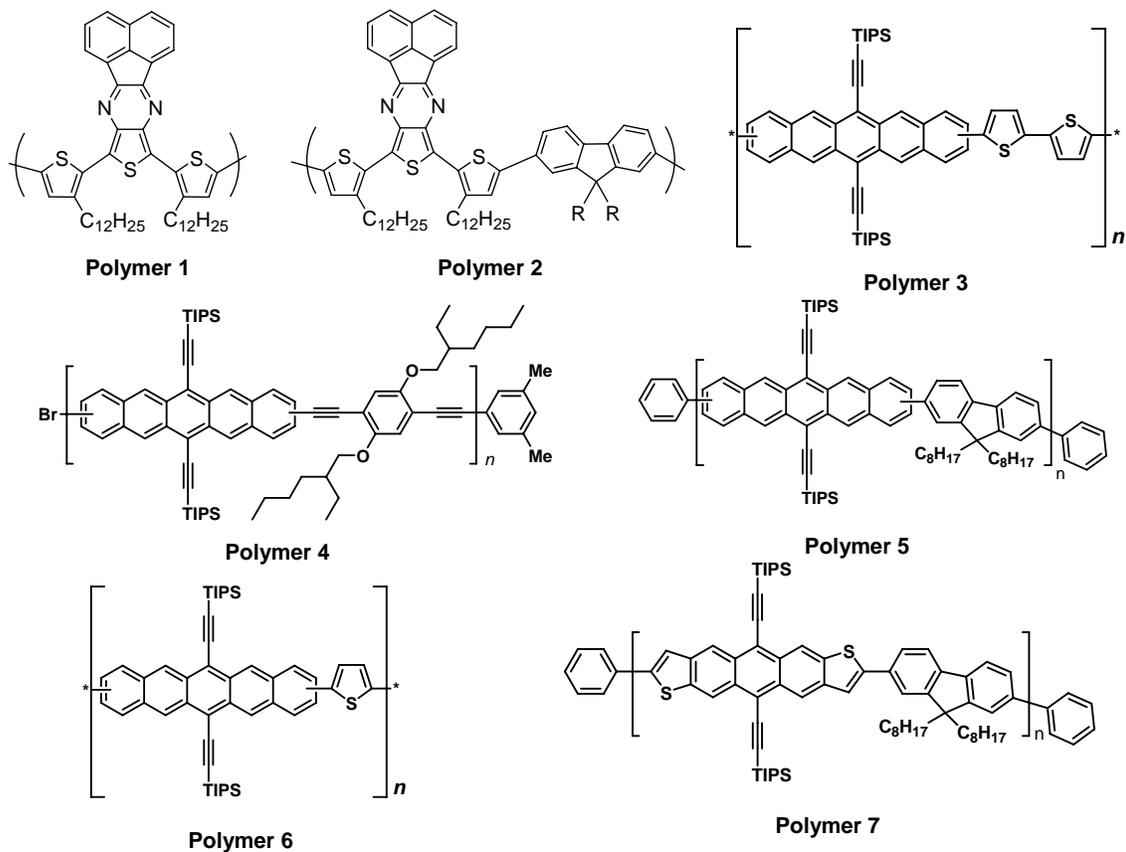
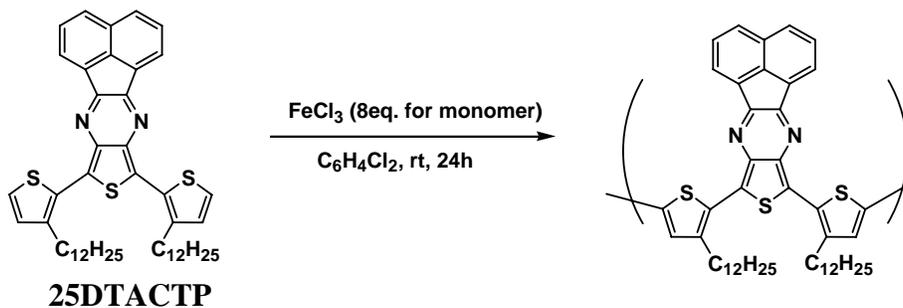**Figure 4.** Chemical structure of low band-gap polymers synthesized.

Polymer 1:

Monomer   synthesis

fuming HNO$_3$
fuming H$_2$SO$_4$
conc.H$_2$SO$_4$

30°C, 3h

Yield = 51.3 %
Pale yellow solid

conc.HCl
Sn powder

20°C-30°C, 6.5h

Yield = 78.8 %
white solid

EtOH, rt, 2 days

Yield = 82.2 %
Yellow solid

2NBS

DMF, -25°C,
2h

Yield =86.0 %
Yellow solid.

NBS

Yield = 95.0 %

1) n-BuLi
2)B(Oi-Pr)$_3$
3)Pinachol

Yield = 84.2 %

Pd(Pph$_3$)$_4$, NaHCO$_3$

DME, 80°C, 20h

Yield = 73.4 %
blue-purple solid

Polymer synthesis

25DTACTP

Mn =1816 , Mw= 1746   Polydispersity=1.04

Solubility:
Partially soluble in THF, Chloroform.

UV-vis spectrum
(Solution: dichlorobenzene and Film: from   dichlorobenzene (drop cast))

Solution
λmax = 329, 455, 740   nm
λonset = 1010 nm (*Eg*=1.23 ev)

Film
λmax = 480, 800   nm
λonset = 1010 nm (*Eg*=1.23 ev)

Polymer 2:

Monomer   synthesis

Yield = 78.7%
Dark blue solid
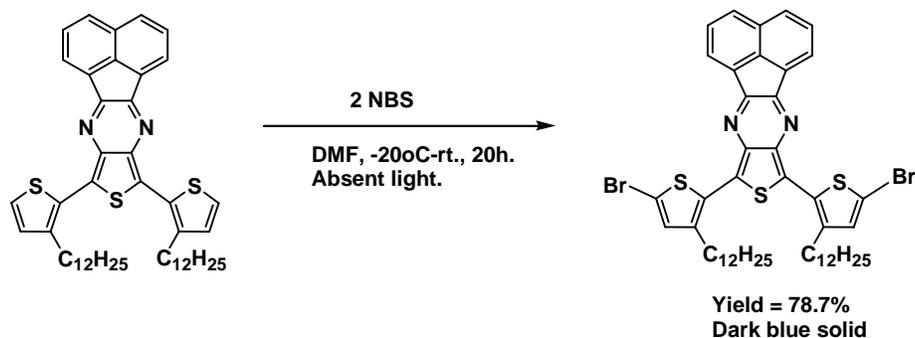
Polymer   synthesis
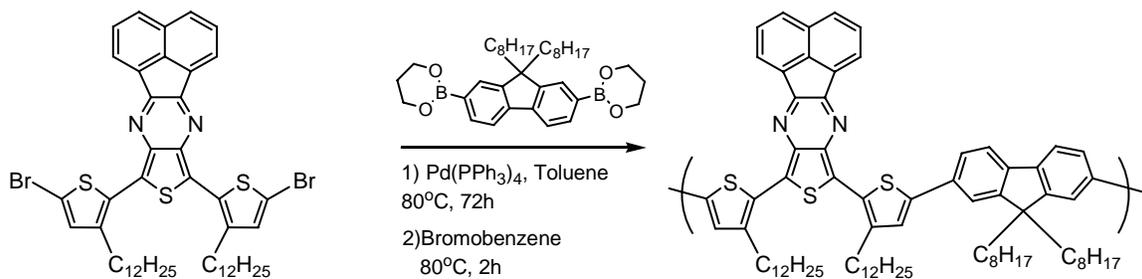
B25DTACTP

Mn =7682, Mw= 14360   Polydispersity=1. 87

Solubility:
Dichlorobenzene 5mg / mL
THF and Chloroform >1mg / mL

HOMO: 5. 04ev   LUMO: 3. 42ev.
 (by cyclic voltammetry, condition; 0.05M tetra-n-butylammonium
hexafluorophosphate(TBAPF$_6$) in o-dichlorobenzene at rt., 100mv sec^{-1}))

UV-vis spectrum
(Solution: dichlorobenzene and Film: from dichlorobenzene (spin cast))

Solution
λmax = 331, 411, 590   nm
$\lambda onset$ = 745 nm
$E gap$ =1.66 ev.

 Film
λmax = 330, 444, 659 nm
$\lambda onset$ = 800 nm

DSC
DSC of the polymer gives a thermal transition around **280°C** which is melting point of
the polymer.

TGA
Td5 = 401.0^{o}C

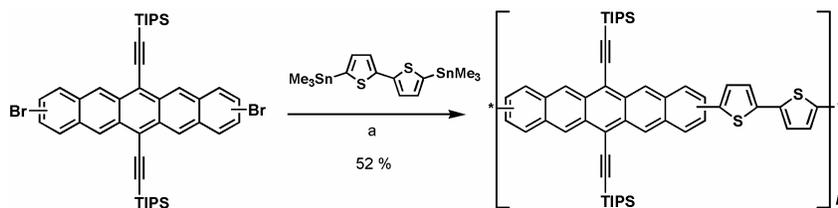# Synthesis of Starting Monomers; TIPSEBr2P and TIPSEBr2DTAnt
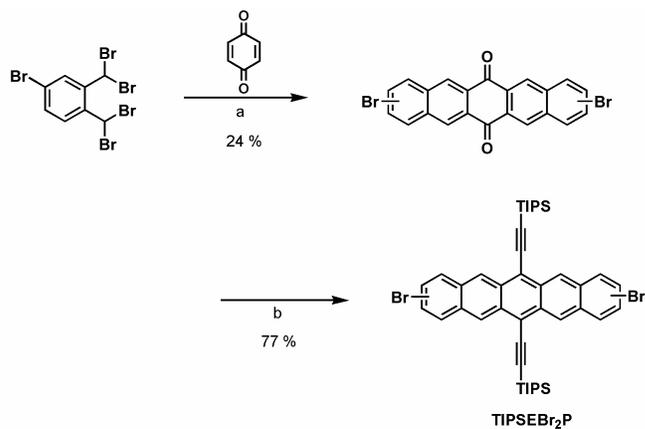
Reagents and Conditions: a) 1,4-Benzoquinone, NaI, DMF, 60°C, 2days, b)1) ^{n}BuLi, TIPSA, THF, rt, overnight, 2) H$_2$O,rt, 3) SnCl$_2$, rt, 3 h.
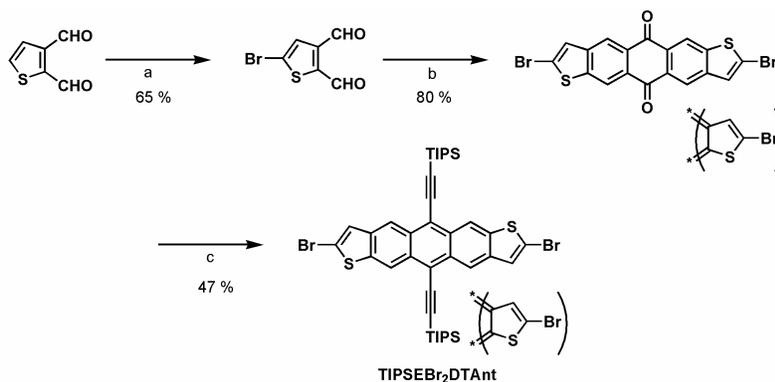
Reagents and Conditions: a) Bromine, Chloroform, rt, overnight, b) 1,4-Cyclohexanedione, 15% KOH aq., EtOH, rt, 3 h. c)1) ^{n}BuLi, TIPSA, Hexane, 60°C, overnight, 2) H$_2$O,rt, 3) SnCl$_2$, HCl, rt.
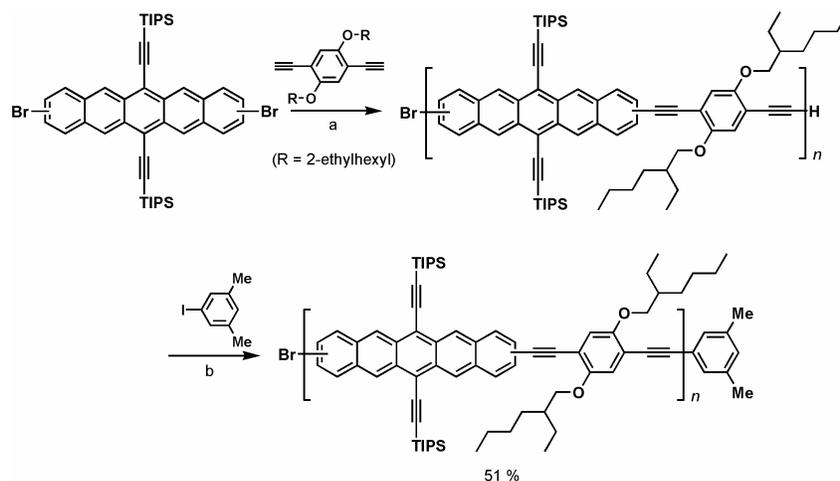
Polymer 3:

Reagents and Conditions: a) Bis(trimethyltin)dithiophene, Pd(PPh$_3$)$_4$,THF, 70 °C, 3 days.

Mn = 2645 , Mw= 3582   Polydispersity= 1.35

Solubility: >10mg/mL in CHCl$_3$, dichlorobenzene.

UV-vis spectrum: λ_{onset} = 789 nm (1.57 eV)

Polymer 4:

Reagents and Conditions: a) Diethynylbenzene, PdCl$_2$(PhCN)$_2$, P^{t}Bu$_3$, CuI, ^{i}Pr$_2$NH, Toluene, rt, 6 h, b) 3,5-Dimethyl-iodobenzene, Ph(PPh$_3$)$_4$, CuI, rt, overnight
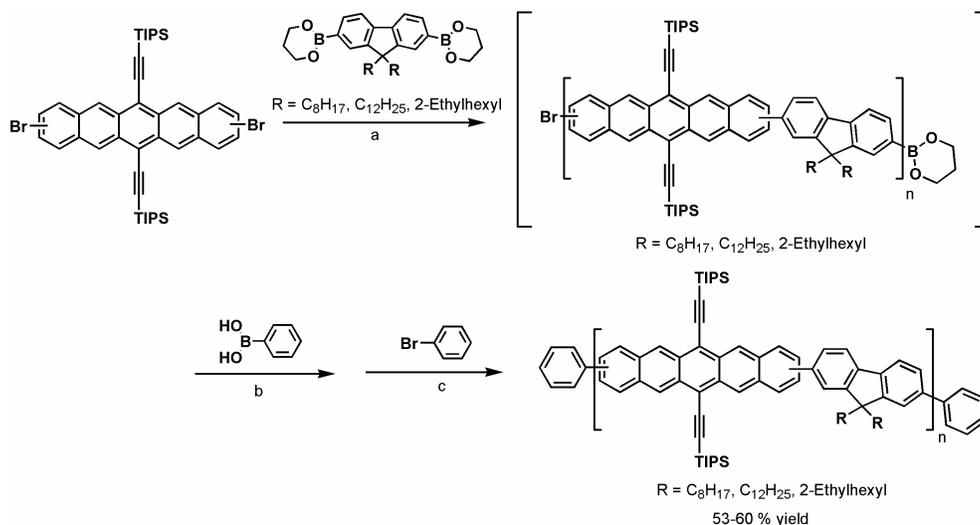
Mn = 16280 , Mw= 41742   Polydispersity= 2.56

Solubility: >10 mg / mL in Chloroform, chlorobenzene, THF and so on

HOMO: -5.24 eV   LUMO: -3.54 eV

UV-vis spectrum: λ_{onset} = 695 nm (1.78 eV, ODCB), 706 nm (1.76 eV, Film)
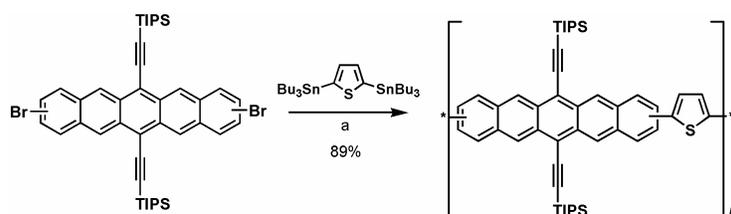
$T_{decomp.} = \sim 400\ ^o$C

Polymer 5:

Reagents and Conditions: a) Fluorene diboron, Pd(PPh$_3$)$_4$, 2 M K$_2$CO$_3$, Aliquat 336, Toluene, 75-80 °C, 1 - 3 days, b) Phenylboronic acid, 2 h, 80 °C, c) bromobenzene, 2 h, 80 °C.

R = C$_{12}$H$_{25}$; Mn = 12342 , Mw= 27959   Polydispersity= 2.265

R = C$_{12}$H$_{25}$; Solubility: > 10 mg/mL in hexanes, THF, chloroform

R = C$_8$H$_{17}$; UV-vis spectrum: λ_{onset} = 693 nm (1.79 eV, ODCB), 694 nm (1.79 eV, Film)

Polymer 6:

Reagents and Conditions: a) Bis(trimethyltin)dithiophene, Pd(PPh$_3$)$_4$,THF, 70 °C, 3 days.
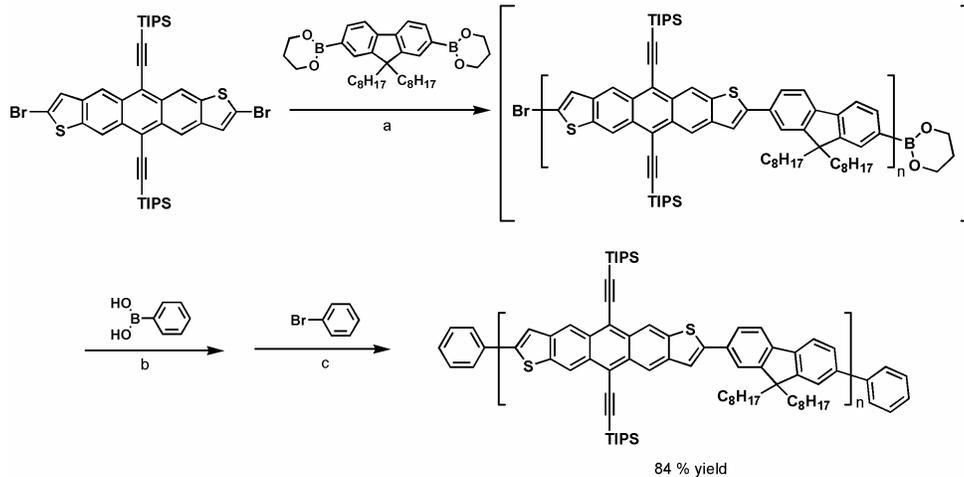
Mn = 3181, Mw= 6342, Polydispersity= 1.99

Solubility: >10mg/mL in CHCl$_3$, dichlorobenzene.

HOMO: -5.01 eV   LUMO: -3.50 eV (calculated from UV-vis onset)

UV-vis spectrum: λ_{onset} = 819 nm (1.51 eV)

Polymer 7:

Reagents and Conditions: a) Fluorene diboron, Pd(PPh$_3$)$_4$, 2 M K$_2$CO$_3$, Aliquat 336, Toluene, 80-85 °C, 3 days, b) Phenylboronic acid, 2 h, 80 °C, c) bromobenzene, 2 h, 80 °C.

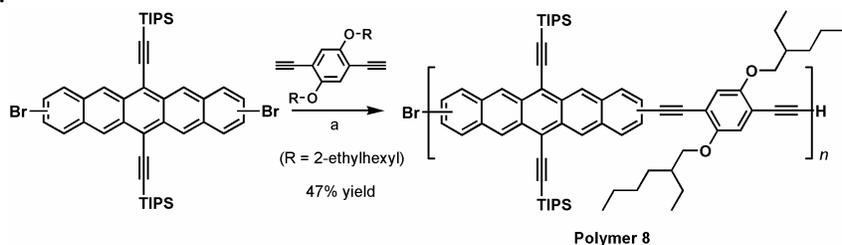Molecular weight could not be determined due to bad solubility in THF

Solubility: 5 mg / mL in chlorobenzene

HOMO: -5.30 eV   LUMO: -3.38 eV

UV-vis spectrum: λ_{onset} = 607 nm (2.04 eV, ODCB), 626 nm (1.98 eV, Film)

Polymer 8:

Polymer 8

Reagents and Conditions: a) Diethynylbenzene, PdCl$_2$(PhCN)$_2$, P^{t}Bu$_3$, CuI, ^{i}Pr$_2$NH, Toluene, rt, 2 days.

Mn = 23921 , Mw= 57836   Polydispersity= 2.418

Solubility: .>10 mg/mL in chloroform, dichlorobenzene

HOMO: -5.24 eV   LUMO: -3.54 eV

UV-vis spectrum: λ_{onset} = 695 nm (1.78 eV, ODCB), 706 nm (1.76 eV, Film)

$T_{decomp.}$ = ~ 400 °C

PV performance of poly(DOF-25DTACTP) (polymer 2)

Solar cells incorporating the low bandgap polymer poly(DOF-25DTACTP) were fabricated by dissolving 12.5 mg of the polymer and 12.5 mg of phenyl-c61-butyric acid methyl ester (PCBM)into 1 mL of *ortho*-dichlorobenzene (ODCB). This solution was then spun onto the transparent conductor, indium-tin-oxide (ITO) coated with poly(3,4-ethylenedioxythiophene) poly(styrene sulfanate) (PEDOT:PSS) and then allowed to dry overnight before 100 nm of Al was deposited in a high vacuum.

Figure 5 compares the solar cell performance of optimized poly(DOF-25DTACTP):PCBM blends spun from chlorobenzene (CB) and *ortho*-dichlorobenzene (ODCB). The lower current in the poly(DOF-25DTACTP):PCBM spun from CB comes from the lower mobility associated with this more quickly drying solvent, which has been observed in polythiophenes. [Li et al. 2005] However, in contrast to P3HT:PCBM the current is much lower due to a poor absorption coefficient. While poorly understood, the donor-acceptor, or push-pull synthetic approach of low bandgap polymers can lead to a low absorption coefficient due to weak wavefunction overlap. In spite of this, cells incorporating this low gap polymer had an open-circuit voltage and fill factor very similar to the P3HT:PCBM cells. [Li et al. 2005] The overall efficiencies of the two devices are 4.4 and 0.75%. Current efforts are aimed at maintaining the open-circuit voltage and fill factor while increasing the absorption coefficient and further investigating the optical properties of low gap polymers synthesized using the push-pull strategy.
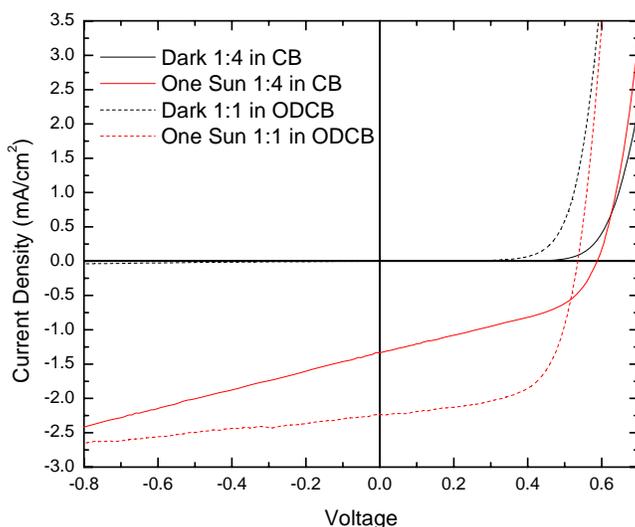

Figure 5. Solar cell performance of optimized poly(DOF-25DTACTP):PCBM blends spun from chlorobenzene (CB) and *ortho*-dichlorobenzene (ODCB).

Publications:
S. R. Scully, M. D. McGehee, **J. Appl. Phys.** 2006, 100, 034907.
S. R. Scully, P. B. Armstrong, C. Edder, J. M. J. Fréchet, and M. D. McGehee *submitted*
T. Okamoto, M.L. Senatore, M.M. Ling, A.B. Mallik, M.L. Tang, Z. Bao, **Adv. Mater**.
in press.

References:

1. Kippelen, B., Yoo, S. & Domercq, B. Efficient thin-film organic solar cells based on pentacene/C60 heterojunctions. Appl. Phys. Lett. 85, 5427-5429 (2004).
2. Hsiang-Lin, Y., Tien-Sung, L., Weissman, S. I. & Sloop, D. J. Time resolved studies of pentacene triplets by electron spin echo spectroscopy. Journal of Chemical Physics 80, 102-107 (1984).
3. Jundt, C. et al. Exciton Dynamics in Pentacene Thin Films Studied by Pump-Probe Spectroscopy. Chem. Phys. Lett 241, 84-88 (1995).
4. Liu, Y. X., Summers, M. A., Edder, C., Fréchet, J. M. J., McGehee, M.D. Using Resonance Energy Transfer to Improve Exciton Harvesting in Organic-Inorganic Hybrid Photovoltaic Cells. Advanced Materials 17, 2960-2964 (2005).
5. Kuhn, H. J. Chem. Phys. J. Chem. Phys. 53, 101 (1970).
6. Scully, S. R. & McGehee, M. D. Effects of optical interference and energy transfer on exciton diffusion length measurements in organic semiconductors. Journal of Applied Physics 100, 034907 (2006).
7. CA is the acceptor chomophore density which is also used in the calculation of Ro, since Ro depends on the molecular absorptivity. Presented a different way we could show that the rate depends only on the total absorption coefficient. As formulated CA must be consistently used in this equation and in the calculation of Ro. We choose 8/nm3.
8. Liu, Y. X., Summers, M. A., Scully, S. R. & McGehee, M. D. Resonance energy transfer from organic chromophores to fullerene molecules. Journal of Applied Physics 99, 93521-1 (2006).
9. Edder, C., Armstrong, P. B., Prado, K. B. & Frechet, J. M. J. Benzothiadiazole-and pyrrole-based polymers bearing thermally cleavable solubilizing groups as precursors for low bandgap polymers. Chemical Communications, 1965-1967 (2006).
10. Forster, T. Transfer Mechanisms of Electronic Excitation. Discussions Faraday Soc. 27, 7 (1959).
11. Theander, M. et al. Photoluminescence Quenching at a Polythiophene/C_{60} Heterojunction. Phys. Rev. B 61, 12957-63 (2000).
12. Pope, M. & Swenberg, C. E. Electronic processes in organic crystals (Clarendon Press, Oxford, 1982).
13. Haugeneder, A. et al. Exciton diffusion and dissociation in conjugated polymer fullerene blends and heterostructures. Physical Review B 59, 15346-15351 (1999).

14. G. Li, V. Shrotriya, J. Huang, Y. Yao, T. Moriarty, K. Emery, and Y. Yang, Nat. Mater. 2005, **4**, 864.

Contacts
zbao@stanford.edu
mmcgehee@stanford.edu